Catal Lett (2012) 142:131–137
DOI 10.1007/s10562-011-0739-3

Effects of Zr and K Promoters on Precipitated Iron-Based Catalysts for Fischer–Tropsch Synthesis

Haojian Zhang · Hongfang Ma · Haitao Zhang · Weiyong Ying · Dingye Fang

Received: 3 September 2011 / Accepted: 4 November 2011 / Published online: 17 November 2011

Abstract The effects of Zr and K promoters on the structure, adsorption, reduction, carburization and catalytic behavior of precipitated iron-based Fischer–Tropsch synthesis (FTS) catalysts were investigated. The catalysts were characterized by N_2 physisorption, temperature-programmed reduction/desorption (TPR/TPD) and Mössbauer effect spectroscopy (MES) techniques. As revealed by N_2 physisorption, Zr and/or K promoted catalysts showed lower surface area than Fe/SiO_2 catalyst. Zr promoter inhibited the reduction and carburization because of the interaction between Fe and Zr in $Fe–Zr/SiO_2$ catalysts. K promoter enhanced the reduction in CO and apparently facilitated the CO adsorption, thus promoted the carburization, but it retarded the reduction in H_2 and severely suppressed the H_2 adsorption. Compared with the singly promoted catalysts, the doubly promoted catalyst had the highest FTS activity. In addition, both Zr and K promoters suppressed the formation of methane and shifted the production distribution to heavy hydrocarbons.

Keywords Fischer–Tropsch synthesis · Precipitated iron-based catalyst · Zr promoter · K promoter

1 Introduction

Fischer–Tropsch synthesis (FTS) is an alternative route for the production of clean liquid fuels and other chemicals from syngas ($CO + H_2$) derived from coal, natural gas or biomass. Due to the limited supplement and unpredictable price of crude oil, an increasing attention has been renewedly focused on FTS in academic or industrial research than before in recent years. This situation is especially obvious in the countries with abundant coal reserves and a shortage of other sources of energy, such as the USA, China, India, Australia, and South Africa [1]. The iron-based catalysts are often used in commercial operations, due to their low cost, high FTS activity as well as high water–gas-shift (WGS) activity, which helps to make up the deficit of H_2 in the syngas from coal gasification [2, 3].

In order to obtain excellent performances (activity, selectivity and stability) of iron-based catalysts, lots of efforts have been made on the addition of electronic or structural promoters [4]. Typical iron-based FTS catalysts contain more or less potassium as an electronic promoter. It is believed that K promotes the formation of olefins and longer-chain hydrocarbon molecules, the carburization of surface Fe, and suppresses the formation of CH_4 [5–8]. Also K strengthens the Fe–C bond by increasing the electron density on Fe while weakening Fe–H and C–O bonds[8, 9].The effect of K on the catalytic behavior of iron-based FTS catalysts has been extensively investigated over various catalyst systems [5–8, 10–13]. Most of these studies showed that the FTS activity of modified catalyst either increases [7] or passes through a maximum as a function of K loading [5, 6, 8, 10, 11]. Enhanced WGS activity on K-promoted iron-based catalysts also has been observed [6, 7].

Zirconium has attracted considerable scientific interests for its potential use as a catalyst promoter. The effect of Zr promoter on catalytic behavior of cobalt-based FTS catalysts has been widely investigated [14–18]. However, systematical studies of Zr in iron-based FTS catalysts are

H. Zhang · H. Ma · H. Zhang · W. Ying (✉) · D. Fang
State Key Laboratory of Chemical Engineering, Engineering Research Center of Large Scale Reactor Engineering and Technology of the Ministry of Education, East China University of Science and Technology, 200237 Shanghai, China
e-mail: wying@ecust.edu.cn

so limited [19, 20]. Although O'Brien et al. [19] investigated the effects of Zr promoter on ultrafine iron oxide catalyst, its influence on FTS product distribution was not clear. Recent work done by Lohithern et al. [20] indicated that Zr improved the activity of 100Fe/5Cu/17SiO_2 catalyst, but the evaluating conditions were rather modest. Also, there is considerable interest in the development of more sulfur tolerant catalysts, as many FTS catalysts suffer rapid and substantial loss of activity by poisoning in the presence of sulfur at ppm levels. Miyamoto et al. [21] reported that Zr modified catalyst showed high sulfur resistance.

Though Zr and K promoters have been widely used and investigated, no study has illustrated the individual and synergistic effects of Zr and K promoters on precipitated iron-based catalysts. In the present work, four catalysts (100Fe/12SiO_2, 100Fe–1Zr/12SiO_2, 100Fe–3K/12SiO_2 and 100Fe–1Zr–3K/12SiO_2) were prepared to investigate the effects of Zr and K promoters on the FTS performances. Temperature-programmed reduction/desorption (TPR/TPD) and Mössbauer effect spectroscopy (MES) were used to elucidate how Zr and K promoters affected the reduction and carburization behaviors of iron-based catalysts. The FTS activity, stability and hydrocarbon product distribution were investigated and correlated with the characterization results of catalysts.

2 Experimental

2.1 Catalyst Preparation

The catalysts used in this study were prepared by a combination of precipitation, spry drying and impregnation techniques. Briefly, a solution containing $Fe(NO_3)_3$, SiO_2 sol with an Fe/Si atomic ratio of 100/12 was introduced into a continuously stirred flask together with a NH_4OH solution for the precipitation at 70 ± 1 °C and pH value of 8.0–9.0. After precipitation, the precipitate was filtered and washed thoroughly with deionized water. Then the required amount of K_2CO_3 solution and deionized water were added into the filter cake to obtain the desired atomic ratio of 100Fe–x(x = 0 or 3)K/12SiO_2. The slurry was spray dried, and then the appropriate sample was impregnated with $Zr(NO_3)_4$ to obtain the atomic ratio of 100Fe–1Zr–x(x = 0 or 3)K/12SiO_2. The obtained catalysts were calcined at 500 °C for 5 h. The 100Fe/12SiO_2 and 100Fe/3K/12SiO_2 catalysts were prepared with the same method. The final fresh catalysts were 100Fe/12SiO_2, 100Fe–1Zr/12SiO_2, 100Fe–3K/12SiO_2 and 100Fe–1Zr–3K/12SiO_2 in atomic ratio, which were labeled as Fe/SiO_2, Fe–Zr/SiO_2, Fe–K/SiO_2 and Fe–Zr–K/SiO_2, respectively. In all tests, the catalysts were pressed into pellets, crushed and sieved to retain 20-40 mesh particles prior to loading to a fixed bed reactor. The detailed composition and nomenclature are presented in Table 1.

2.2 Catalyst Characterization

The composition of the catalysts was determined by sequential X-ray fluorescence spectrometer (XRF) using a LAB CENTER XRF-1800(Shimadzu, Japan).

The BET surface area, pore volume and pore size distribution of the fresh catalysts were measured by N_2 physisorption at −196 °C using Micromeritics ASAP 2020 automated system. Each sample was degassed under a vacuum of 10^{-3} mm Hg at 100 °C for 1 h, after which the temperature was raised to 300 °C (at a rate of 10 °C/min) and held for 2 h before N_2 adsorption.

TPR experiments were performed on Micromeritics Auto chemisorption analyzer 2920. Typically, about 40 mg catalyst was loaded into a U-type quartz tube reactor and ramped from room temperature to 900 °C in 10% H_2/90% Ar(H_2-TPR) or 5% CO/95% He(CO-TPR). The heating rate was maintained at 10 °C/min and the flow rate of reduction gas was 50 mL/min. The variation of the reducing gas concentration was monitored by a thermal conductivity detector (TCD). Isopropyl alcohol gel (−88 °C) and liquid nitrogen trap were respectively used to remove water(H_2-TPR) and CO_2(CO-TPR) formed during tests.

The H_2- and CO-TPD experiments were performed in the same system as used in TPR. H_2-TPD was used to measure the hydrogen adsorption and desorption on H_2-reduced catalysts. For H_2-TPD on H_2-reduced catalysts, the catalyst sample (200 mg) was firstly reduced in pure H_2 (50 mL/min) at 400 °C for 4 h and then cooled to 50 °C.

Table 1 BET results of the fresh catalysts

Catalysts	Analyzed composition (by atomic ratio)	Surface area (m^2/g)	Pore volume (cm^3/g)	Average pore size (nm)
Fe/SiO_2	100Fe/13.2SiO_2	231	0.45	6.38
Fe–Zr/SiO_2	100Fe–1.6Zr/13.5SiO_2	200	0.42	6.86
Fe–K/SiO_2	100Fe–3.0K/13.4SiO_2	187	0.41	6.96
Fe–Zr–K/SiO_2	100Fe–1.4Zr–3.0K/13.5SiO_2	193	0.41	6.74

After that, the reduced sample was purged with Ar until the baseline of H_2 signal leveled off. Finally, the sample was heated to 700 °C at ramp of 10 °C/min and kept for 30 min. CO-TPD was used to measure the CO adsorption and desorption behavior on carburized catalysts. The catalyst sample (50 mg) was firstly carburized in 5%CO/95%He (50 mL/min) at 300 °C for 5 h and cooled to 50 °C. Then, the carburized sample was purged with He until the baseline of CO signal leveled off. Finally, the temperature was increased to 800 °C at ramp of 10 °C/min.

The Mössbauer spectra of catalysts were recorded at room temperature using a Wissel constant acceleration Mössbauer spectrometer (Germany) with a ^{57}Co(Pd) source. The spectra were collected over 512 channels in the mirror image format. Data analysis was performed using a nonlinear least square fitting routine that models the spectra as a combination of singlets, quadruple doublets and magnetic sextuplets based on a Lorentzian line shape profile. The components were identified based on their isomer shift (IS), quadruple splitting (QS) and magnetic hyperfine field (Hhf). Magnetic hyperfine fields were calibrated with the 330kOe field of α-Fe at ambient temperature. A selected sample was also measured at low temperature (−258 °C).

2.3 Catalyst Evaluation

Catalysts prepared were tested in a 1 cm i.d. stainless steel fixed bed reactor with an effective bed length of approximately 10 cm. The feed gas with a H_2/CO ratio of 0.67 passed through an activated charcoal trap, an oxygen-removal trap and a silica-gel/5A molecular sieve trap to remove tiny amounts of metal carbonyls, oxygen and water before entering the reactor. The flow rate of the purified syngas was controlled by a mass flow controller (Brooks, 5850E). The outlet of the reactor was connected with a hot trap (150 °C) and a cold trap (0 °C) under system pressure. The pressure of the tail gas was released through a Tescom backpressure regulator. Before reaction, catalysts were pretreated in situ with syngas ($H_2/CO = 0.67$) at 280 °C, 0.25 MPa, 1.0NL/g-cat/h for 24 h. Following catalyst pretreatment, the reactor was adjusted to reaction conditions of 270 °C, 1.50 MPa, 1.0NL/g-cat/h and $H_2/CO = 0.67$.

Characterization of the catalysts after reduction and reaction required proper passivation before exposure to air [16]. After each reduction or reaction completed, catalyst was cooled down to room temperature under N_2. Then passivation was done by introducing a flow rate of 40 mL/min of 1% O_2 in N_2 to the catalyst. Finally the catalyst was coated with paraffin wax for preventing the oxidation and then sealed for characterization.

3 Results and Discussion

3.1 BET Surface Area and Pore Size Distribution

The BET surface area, pore volume and average pore size of the fresh catalysts are illustrated in Table 1. As shown in Table 1, all of the catalysts possess high BET surface area (187–231 m^2/g) due to the incorporation of precipitated SiO_2. Many previous studies have proved that addition of precipitated SiO_2 results in higher surface area [22, 23]. It is evident that Zr and/or K promoted catalysts show lower BET area and pore volume but larger average pore size than those of Fe/SiO_2 catalyst. A possible reason for the increase in average pore size of Zr and/or K promoted catalysts is that the small pores of catalyst precursor were blocked when Zr and/or K was added.

3.2 Reduction and Carburization Behaviors

The effects of Zr and K promoters on the reduction and carburization behaviors of the catalysts were investigated by H_2-TPR and CO-TPR. The profiles of H_2-TPR and CO-TPR are presented in Figs. 1 and 2, respectively. As shown in Fig. 1, there are two apparent reduction stages on catalysts in the temperature range of 300–900 °C. The first stage is related to the reduction of $Fe_2O_3 \rightarrow Fe_3O_4$ and $Fe_3O_4 \rightarrow FeO$, meanwhile the second stage is ascribed to the reduction of $Fe_3O_4 \rightarrow FeO$ and $FeO \rightarrow Fe$ [4, 24, 25]. The existence of FeO at the first stage in H_2-TPR for the catalysts incorporated with SiO_2 has been reported by many studies [23, 26]. It is reasonable to suppose that the FeO is stabilized by the support. The H_2-TPR profiles clearly indicate that the reduction peaks of Zr and/or K promoted catalysts shift to higher temperature in contrast with Fe/SiO_2 catalyst. This result may suggest a strong

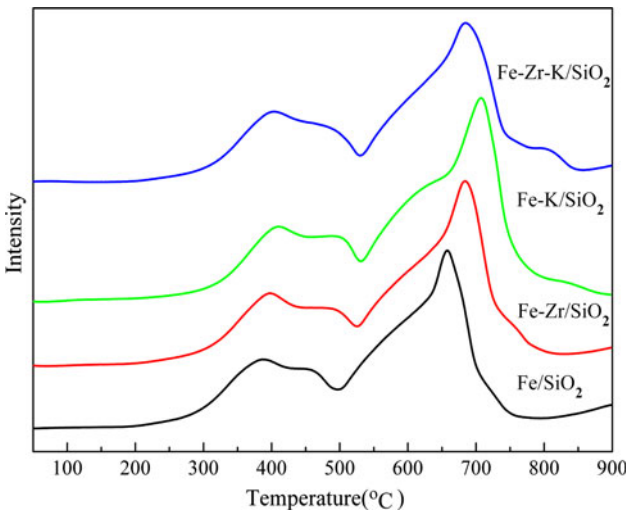

Fig. 1 H_2-TPR profiles of the catalysts

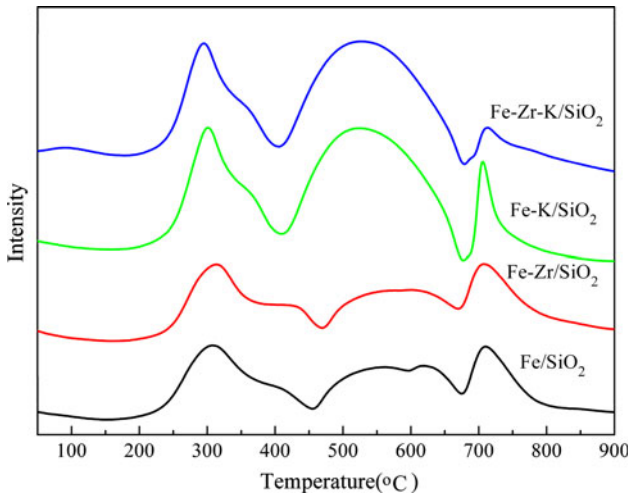

Fig. 2 CO-TPR profiles of the catalysts

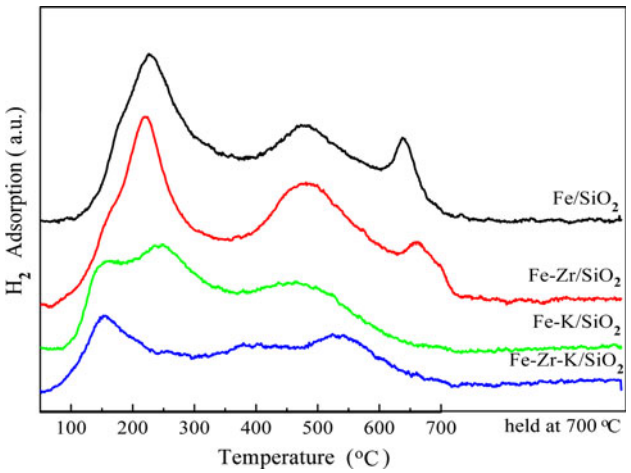

Fig. 3 H_2-TPD profiles of the catalysts

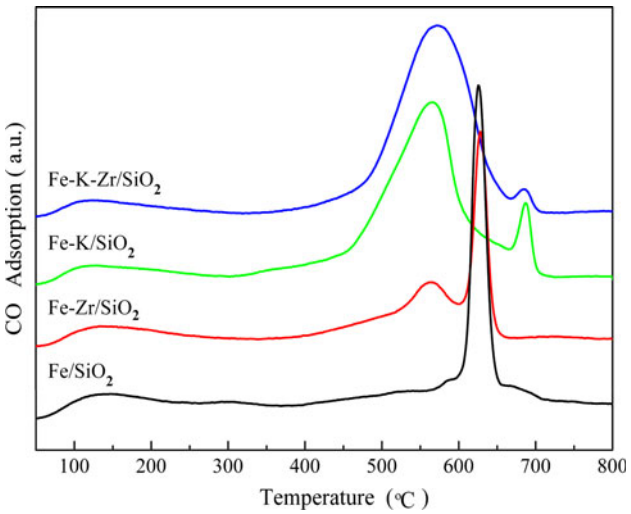

Fig. 4 CO-TPD profiles of the catalysts

interaction between Fe and Zr in Fe–Zr/SiO_2 catalyst [27]. As an alkali promoter, K inhibits the dissociative adsorption of H_2. Thus, the reduction of K promoted catalysts in H_2 atmosphere is suppressed.

Figure 2 shows the CO-TPR profiles of the catalysts. There are three well-separated peaks in CO-TPR profiles for all catalysts. The first peak is ascribed to the reduction of Fe_2O_3–Fe_3O_4. The second peak is corresponding to the carburization of iron oxides, and the peak after 650 °C is corresponding to the carburization of the difficultly reduced iron oxide phase [28]. From the CO-TPR profiles of catalysts without K promoter, it is clearly that the Zr promoter suppresses the reduction/carburization to some extent. Obviously, the addition of K promoter has a marked effect on reduction/carburization. That is K promoter moves the reduction/carburization peaks to lower temperature and strengthens the peaks intensity greatly. Compared with Fe–K/SiO_2 catalyst, the first peak shifts to lower temperature and the area of the third peak becomes smaller for Fe–Zr–K/SiO_2 catalyst. These results indicate that coexistence of Zr and K promoters leads to easier carburization.

3.3 H_2 and CO Chemisorptions

H_2-TPD is used to qualitatively reflect the H_2 adsorption behavior of catalysts. As illustrated in Fig. 3, the H_2-TPD curves of Fe/SiO_2 and Fe–Zr/SiO_2 show no apparent difference in the peak style and position. It is clear that the TPD curves of Fe/SiO_2 and Fe–Zr/SiO_2 catalysts show an intense peak at about 220 °C and a group of peaks at above 400 °C. The figure also shows that K promoter eliminates the adsorption peak at high temperature (>600 °C). Obviously, addition of K not only suppresses the adsorption of H_2, but also shifts the adsorption peak to lower temperature. H_2 desorption peaks below 250 °C are corresponding to the H species adsorbed on the metallic iron surface. The peaks at higher temperature (>350 °C) may be ascribed to the cleavage of OH species on the difficultly reduced oxide surface in catalysts [29]. H_2-TPD results indicate that K apparently suppresses the H_2 adsorption on catalyst surfaces. It is consistent with report that K is a very strong poison for H_2 dissociation [30].

Figure 4 illustrates the CO-TPD profiles of CO-carburized catalysts. As illustrated in Fig. 4, the CO desorption peaks of catalysts all locate in temperature range of 450–700 °C. For Fe/SiO_2 catalyst, the CO-TPD curve demonstrates a sharp peak at 625 °C. With the addition of Zr promoter individually, there are a sharp peak at 625 °C and a broad peak at lower temperature for Fe–Zr/SiO_2. Both Fe–K/SiO_2 and Fe–Zr–K/SiO_2 show a broad peak at 550°C and a more intense peak at about 685 °C. Clearly,

the CO desorption peak intensity increases obviously with the addition of K promoter. However, when Zr coexists with K in catalyst, the extent of CO adsorption can be further increased. This phenomenon has been rarely reported in previous studies. Also, there are few works studying on the CO adsorption on iron carbide surfaces [29, 31]. The desorption temperatures of CO on carburized catalysts are close to that of the dissociative CO. If desorbed in thermal flashing, the required temperature for CO on iron carbide surfaces should be about 500 °C, which is slightly lower than the CO desorption temperatures in our study. Therefore, the CO-TPD peaks on carburized catalysts are most likely to result from the strongly bound CO on iron carbide surfaces [29].These results imply that K largely improves the CO adsorption on carburized catalysts, which is in good consistence with the effect of K on CO adsorption on iron surfaces [32].

3.4 Crystallite Structure of the Catalysts after Activation and FTS Reaction

Mössbauer spectra can provide quantitative information on the content of the iron-phase composition [6]. Table 2 lists the iron-phase composition of the catalysts by fitting the Mössbauer spectra. Clearly, it can be seen that the detected iron phases in the catalysts at two different states include Fe_3O_4, FeC_x, Fe^{3+}(spm) and Fe^{2+}(spm). Superparamagnetic(spm) refers to iron phases located in small particles with diameter less than 13.5 nm [33]. It is found that the content of carbide in reduced catalysts increases in the order of Fe–Zr/SiO_2, Fe/SiO_2, Fe–K/SiO_2 and Fe–Zr–K/SiO_2. This result indicates that the carburization of Fe–Zr/SiO_2 is suppressed as the interaction between Fe and Zr, while that of K promoted and doubly promoted catalysts is promoted, which is consistent with the results of TPR and TPD.

After reaction for 200 h, the content of iron carbide in used catalysts increases as compared with that in the reduced catalysts, indicating that the catalysts were further reduced and carburized in the process of FTS reaction. Moreover, the content of iron carbide in the used catalysts is in similar trends with that of reduced catalysts. The carburization extent of Fe–Zr–K/SiO_2 is the highest, while that of Fe–Zr/SiO_2 is the lowest.

In order to accurately understand the nature of the spm phases, the reduced Fe–Zr–K/SiO_2 catalyst was measured by MES at low temperature (−258 °C). Compositions of the reduced catalyst tested under room and low temperatures are listed in Table 3. Obviously, the reduced sample includes Fe_3O_4, FeC_x and α-Fe, and the spm phases disappear at −258 °C. The result implies that the spm phases in the catalyst are the mixture of Fe_3O_4, α-Fe and FeC_x, which is consistent with the study of Cui et al. [34].

Table 2 Iron phase compositions of catalysts at different states

Catalysts	After reduction		After reaction	
	Phases	Area (%)	Phases	Area (%)
Fe/SiO_2	Fe^{3+}	66.5	Fe^{3+}	33.1
	Fe^{2+}	3.7	Fe^{2+}	1.0
	Fe_3O_4(A)	4.3	Fe_3O_4(A)	12
	Fe_3O_4(B)	8.9	Fe_3O_4(B)	33.2
	FeC_x	16.6	FeC_x	20.7
Fe–Zr/SiO_2	Fe^{3+}	66.2	Fe^{3+}	33.7
	Fe^{2+}	4.5	Fe^{2+}	4.3
	Fe_3O_4(A)	5.8	Fe_3O_4(A)	12.9
	Fe_3O_4(B)	10.8	Fe_3O_4(B)	26.4
	FeC_x	12.7	FeC_x	18.7
Fe–K/SiO_2	Fe^{3+}	75.5	Fe^{3+}	36.2
	Fe^{2+}	5.8	Fe^{2+}	7.3
	FeC_x	18.7	Fe_3O_4(A)	8.5
			Fe_3O_4(B)	22.9
			FeC_x	25.1
Fe–Zr–K/SiO_2	Fe^{3+}	72.8	Fe^{3+}	51
	Fe^{2+}	6.9	Fe^{2+}	2.3
	FeC_x	20.3	Fe_3O_4(A)	5.1
			Fe_3O_4(B)	10.3
			FeC_x	31.3

3.5 FTS Performances of the Catalysts

The FTS performances of catalysts were measured in a fixed bed reactor under reaction conditions of 270 °C, 1.50 MPa, 1.0NL/g-cat/h and $H_2/CO = 0.67$. The activities, stabilities and product selectivities were tested over a period of 200 h steady-state runs.

3.5.1 Activity and Stability

The results of the effects of Zr and K promoters on activity and stability are shown in Fig. 5 and Table 4, respectively.

Table 3 Iron phase compositions of reduced Fe–Zr–K/SiO_2 catalyst under room and low temperatures

Test conditions	Phases	Area(%)
Room temperature	Fe^{3+}	72.8
	Fe^{2+}	6.9
	FeC_x	20.3
Low temperature (−258 °C)	Fe_3O_4(A)	23.3
	Fe_3O_4(B)	47.5
	FeC_x	21.3
	α-Fe	7.9

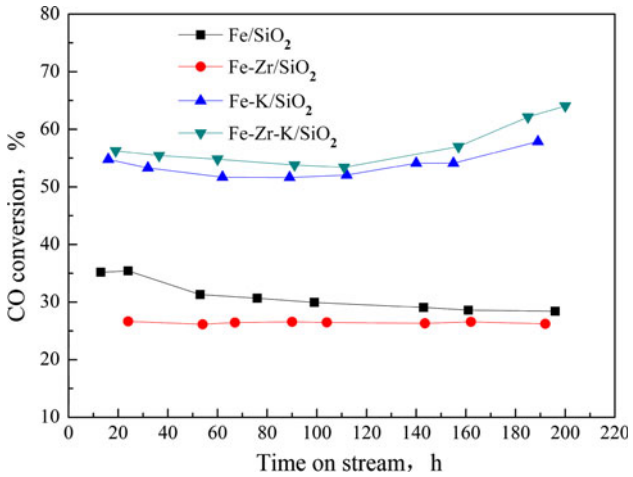

Fig. 5 CO conversion of the catalysts. Reaction conditions: 270 °C, 1.50 MPa, 1.0NL/g-cat/h and $H_2/CO = 0.67$

It is evident that there is no obvious deactivation for all these catalysts except for Fe/SiO_2 catalyst during the 200 h FTS reaction. For the unpromoted Fe/SiO_2, the CO conversion is at a low level (35%) at the beginning of the reaction, but gradually decreases with time on stream (TOS) to 28%. For $Fe–Zr/SiO_2$ catalyst, the CO conversion almost remains stable till the end of reaction. In contrast, the CO conversion of $Fe–K/SiO_2$ is initially at a high level (54%), and then gradually increases to 58%. It is worth noting that the CO conversion of $Fe–Zr–K/SiO_2$ keeps nearly at 55% for 140 h, then greatly increases to 66% at the end of reaction. It is generally accepted that iron carbides have been supposed to be the most likely active phases or can have active sites on their surfaces for FTS reaction [35–38]. Therefore, the content of FeC_x can be used to monitor the amount of FTS active sites to some extent. In the present study, there is a clear correlation between the carburization extent and the catalytic activity. The MES results in previous section display that catalyst $Fe–Zr–K/SiO_2$ has the highest amount of FeC_x both after activation and FTS reaction. Thus, the highest activity is obtained on $Fe–Zr–K/SiO_2$ catalyst.

It is well known that a reversible WGS reaction accompanies the FTS reaction on iron-based catalysts [4, 6]. As shown in Table 4, CO_2 selectivity is used as a measure of WGS activity. When incorporated with Zr individually, the CO_2 selectivity of the catalyst is unchanged, but that of the catalysts is enhanced with the addition of K promoter. Our result is consistent with the viewpoint that K promoter can improve the WGS activity [4, 6, 7].

3.5.2 *Product Selectivity*

The hydrocarbon distributions of all catalysts at different TOS are shown in Table 4. It clearly indicates that the selectivity to lower-molecular-weight hydrocarbons (methane and $C_2–C_4$) is suppressed while that to heavy hydrocarbons (C_5^+) is enhanced with the addition of Zr and/or K promoters. The study of Qing et.al [39] also found similar result that addition of Zr decreased methane selectivity and enhanced the C_5^+ hydrocarbons selectivity. In addition, the $C_2^=–C_4^=/C_2^o–C_4^o$ is improved with the corporation of Zr and/or K promoters. It is noteworthy that $Fe–Zr–K/SiO_2$ catalyst has the lowest selectivity to lower-molecular-weight hydrocarbons (methane and $C_2–C_4$) and the highest selectivity to heavy hydrocarbons (C_5^+) among the four catalysts. All of these results imply that the chain propagation reaction is enhanced while the second hydrogenation reaction is suppressed on Zr and/or K promoted catalysts.

Table 4 Activities and selectivities of the catalysts

Catalysts	Fe/SiO_2		$Fe–Zr/SiO_2$		$Fe–K/SiO_2$		$Fe–Zr–K/SiO_2$	
TOS (h)	143	196	144	198	144	200	144	200
Conversion (mol %)								
CO	29.06	28.41	26.31	26.04	54.48	57.61	55.17	66.06
Exit molar H_2/CO ratio	0.42	0.42	0.38	0.39	0.50	0.50	0.49	0.50
$Kp(P_{H2}Pco_2/PcoP_{H2O})$	0.65	0.63	0.51	0.51	18.36	19.74	30.53	31.89
CO_2 selectivity(%,C basis)	33.60	33.28	33.10	33.04	46.96	47.52	46.24	48.03
Hydrocarbon selectivity (wt%)								
CH_4	9.07	9.20	7.88	8.09	6.63	7.02	6.38	5.33
$C_2–C_4$	29.81	29.73	25.73	25.76	21.81	21.89	20.91	17.48
C_5^+	61.12	61.07	66.39	66.15	71.56	71.09	72.71	77.19
$C_2^=–C_4^=/C_2^o–C_4^o$(mol/mol)	2.16	2.12	2.29	2.26	2.36	2.37	2.40	2.38

Reduction conditions: 280 °C, 0.25 MPa, 1.0NL/g-cat/h and $H_2/CO = 0.67$ for 24 h

Reaction conditions: 270 °C, 1.50 MPa, 1.0NL/g-cat/h and $H_2/CO = 0.67$

It has been widely accepted that low exit H_2/CO ratio could facilitate the chain growth reaction [26, 35]. As shown in Table 4, the H_2/CO exit ratio of Fe–Zr/SiO_2 catalyst is lower than that of Fe/SiO_2 catalyst due to the relative low CO conversion. Therefore, high selectivity to heavy hydrocarbons is likely reasonable for Fe–Zr/SiO_2 catalyst. Though the H_2/CO exit ratios of Fe–K/SiO_2 and Fe–Zr–K/SiO_2 are higher, they still have high selectivity to heavy hydrocarbons (C_5^+). This is inconsistent with the effect of H_2/CO ratio on product selectivity. Furthermore, the promoters may affect the hydrocarbon distribution and could cover the effect of H_2/CO ratio [31]. As indicated by H_2-TPD and CO-TPD results, incorporation of K promoter apparently suppresses the H_2 adsorption, and largely enhances the CO adsorption. For Fe–Zr–K/SiO_2 catalyst, the area of H_2-TPD peaks is the smallest, while that of CO-TPD peaks is the largest. Thus, Fe–Zr–K/SiO_2 catalyst has the lowest selectivity to light hydrocarbons and the highest selectivity to heavy hydrocarbons.

4 Conclusions

Zr and K promoters have significant influences on textual properties, adsorption, reduction and carburization behaviors, as well as the FTS performances of iron-based catalysts. Zr and/or K promoted catalysts show lower BET area and pore volume but larger average pore size than those of Fe/SiO_2 catalyst. For Fe–Zr/SiO_2 catalyst, Zr promoter inhibits the reduction and carburization because of the interaction between Fe and Zr. K promoter severely suppresses the H_2 adsorption, but apparently facilitates the CO adsorption, thus promotes the carburization. In the FTS reaction, Fe–Zr–K/SiO_2 catalyst has the highest FTS activity due to the synergistic effect of Zr and K. Meanwhile, both Zr and K can restrain the formation of methane and increase the heavy hydrocarbons selectivity.

Acknowledgments We gratefully acknowledge the financial support from State Key Laboratory of Chemical Engineering (SKL-ChE-09T01).

References

1. Steynberg AP (2004) In: Steynberg AP, Dry ME (eds) Studies in surface science and catalysis, vol. 152, chap. 1, Elsevier, Amsterdam
2. Dry ME (2002) Catal Today 71:227–241
3. Jothmurugesan K, Goodwin JG Jr, Gangwal SK, Spivey JJ (2000) Catal Today 58:335–344
4. Bukur DB, Lang X, Mukesh D, Zimmerman WH, Rosynek MP, Li C (1990) Ind Eng Chem Res 29:1588
5. Dry ME (1981) The Fischer–Tropsch synthesis. Springer-Verlag, New York
6. Yang Y, Xiang HW, Xu YY, Bai L, Li YW (2004) Appl Catal A: Gen 266:181–194
7. Bukur DB, Mukesh D, Patel SA (1990) Ind Eng Chem Res 29:194–204
8. Miller DG, Moskovits M (1988) J Phys Chem 92:6081–6085
9. Dry ME, Shingles T, Boshoff LJ, Oosthuizen GJ (1969) J Catal 15:190–199
10. Ma WP, Kugler EL, Dadyburjor DB (2007) Energy Fuels 21:1832–1842
11. Lohitharn N, Goodwin JG Jr (2008) J Catal 260:7–16
12. Pichler H (1952) In: Frankenberg WG, Komarewsky VI, Rideal EK (eds) Advances in catalysis, vol 4. Academic Press, New York, p 271
13. Dictor RA, Bell AT (1986) J Catal 97:121
14. Ma WP, Ding YJ, Lin LW (2004) Ind Eng Chem Res 43:2391–2398
15. Feller A, Claeys M, van Steen E (1999) J Catal 185:120–130
16. Oukaci R, Sigleton AH, Goodwin JG Jr (1999) Appl Catal A: Gen 186:129–144
17. Ali S, Chen B, Goodwin JG Jr (1995) J Catal 157:35–41
18. Rohr F, Lindvåg OA, Holmen A, Blekkan EA (2000) Catal Today 58:247–254
19. O'Brien RJ, Xu L, Milburn DR, Li Y, Klabunde KJ, Davis BH (1995) Top Catal 2:1–15
20. Lohitharn N, Goodwin JG Jr, Lotero E (2008) J Catla 255:104–113
21. Belosludov RV, Sakahara S, Yajima K, Takami S, Kubo M, Miyamoto A (2002) Appl surf sci 189:245–252
22. Dlamini H, Motjope T, Joorst G, Stege GT, Mdleleni M (2002) Catal Lett 78:201–207
23. Yang Y, Xiang HW, Tian L, Wang H, Zhang CH, Tao ZC, Xu YY, Zhong B, Li YW (2005) Appl Catal A: Gen 284:105–122
24. Jin Y, Datye AK (2000) J Catal 196:8
25. Li S, Li A, Krishnamoorthy S, Iglesia E (2001) Catal Lett 77:197
26. Bukur DB, Sivaraj C (2002) Appl Catal A: Gen 231:201
27. Chen KD, Fan YN, Hu Z, Yan QJ (1996) Catal Lett 36:141
28. Zhao GY, Zhang CH, Qing SD, Xiang HW, Li YW (2008) J Mol Catal A:Chem 286:137–142
29. Zhang CH, Zhao GY, Liu KK, Yang Y, Xiang HW, Li YW (2010) J Mol Catal A:Chem 328:35–43
30. Brown JK, Luntz AC, Schultz PA (1991) J Chem Phys 95:3767–3774
31. Wan HJ, Wu BS, Zhang CH, Xiang HW, Li YW (2008) J Mol Catal A: Chem 283:33–42
32. Cameron SD, Dwyer DJ (1988) Surf Sci 198:315–330
33. Sirmanothan N, Hamdeh HH, Zhang Y, Davis BH (2002) Catal Lett 82:181
34. Cui XJ, Xu J, Zhang CH, Yang Y, Gao P, Wu BS, Li YW (2011) J Catal 282:35–46
35. Zhang CH, Yang Y, Teng BT, Li TZ, Zheng HY, Xiang HW, Li YW (2006) J Catal 237:405–415
36. Riedel T, Schulz H, Schaub G, Jun KW, Hwang JS, Lee KW (2003) Top Catal 26:41
37. Motiope TR, Dlamini HT, Hearne GR, Conville NJ (2002) Catal Today 71:335–341
38. Mansker LD, Jin Y, Bukur DB, Datye AK (1999) Appl Catal A: Gen 186:277
39. Qing M, Yang Y, Wu BS, Xu J, Zhang CH, Gao P, Li YW (2011) J Catal 279:111–122